ACS OMEGA

Article

http://pubs.acs.org/journal/acsodf

Dissolved Selenium(VI) Removal by Zero-Valent Iron under Oxic Conditions: Influence of Sulfate and Nitrate

Soumya Das,* Matthew B. J. Lindsay, Joseph Essilfie-Dughan, and M. Jim Hendry

Department of Geological Sciences, University of Saskatchewan, 114 Science Place, Saskatoon, Canada SK S7N 5E2

Supporting Information

ABSTRACT: Dissolved Se(VI) removal by three commercially available zero-valent irons (ZVIs) was examined in oxic batch experiments under circumneutral pH conditions in the presence and absence of NO_3^- and SO_4^{2-}. Environmentally relevant Se(VI) (1 mg L^{-1}), NO_3^- ([NO_3—N] = 15 mg L^{-1}), and SO_4^{2-} (1800 mg L^{-1}) were employed to simulate mining-impacted waters. Ninety percent of Se(VI) removal was achieved within 4−8 h in the absence of SO_4^{2-} and NO_3^-. A similar Se(VI) removal rate was observed after 10−32 h in the presence of NO_3^-. Dissolved Se(VI) removal rates exhibited the highest decrease in the presence of SO_4^{2-}; 90% of Se(VI) removal was measured after 50−191 h for SO_4^{2-} and after 150−194 h for SO_4^{2-} plus NO_3^- depending on the ZVI tested. Despite differences in removal rates among batches and ZVI materials, Se(VI) removal consistently followed first-order reaction kinetics. Scanning electron microscopy, Raman spectroscopy, and X-ray diffraction analyses of reacted solids showed that Fe(0) present in ZVI undergoes oxidation to magnetite [Fe_3O_4], wüstite [FeO], lepidocrocite [γ-FeOOH], and goethite [α-FeOOH] over time. X-ray absorption near-edge structure spectroscopy indicated that Se(VI) was reduced to Se(IV) and Se(0) during removal. These results demonstrate that ZVI can be effectively used to control Se(VI) concentrations in mining-impacted waters.

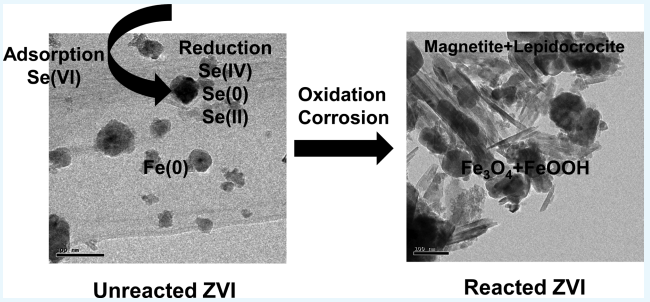

INTRODUCTION

Selenium contamination by anthropogenic activities, including mining, is an increasing environmental issue worldwide.[1−4] Although total dissolved Se rarely exceeds 10 μg L^{-1} in natural waters,[5] concentrations exceeding 100 μg L^{-1} are reported for mining-impacted waters.[4,6] Excessive Se exposure can have negative impacts on aquatic ecosystems.[7] Consequently, the World Health Organization established a 40 μg L^{-1} Se drinking water standard.[8] The corresponding Health Canada and United States Environmental Protection Agency standards are 50 μg L^{-1}.[9,10] Water quality criteria for protection of aquatic life for Se are substantially lower at 1 μg L^{-1} in Canada[11] and 5 μg L^{-1} in the United States.[10]

Selenium contamination by mining and mineral processing is commonly associated with coal operations;[4,7,12] however, Se contamination by copper[6] and uranium[2] mining is also documented. Selenium substitution for sulfur (S) occurs in sulfide minerals, including pyrite [FeS_2], chalcopyrite [$CuFeS_2$], and sphalerite [ZnS].[7,12−14] The oxidative weathering of these sulfides within mine waste deposits can generate sulfate (SO_4^{2-}) and release metals (i.e., Fe, Cu, and Zn) and trace elements, including Se.[15,16] Nitrate (NO_3^-) derived from residual blasting agents can also co-occur with SO_4^{2-}, metals, and trace elements in mining-impacted waters.[17−19] Consequently, Se-bearing waters associated with mining and mineral processing can contain elevated concentrations of Se, SO_4, and NO_3.

Selenium can occur in four oxidation states (i.e., VI, IV, 0, and −II) in the environment; however, Se(VI) and Se(IV) predominate in natural and contaminated waters.[5,7,20] Se(VI) oxyanions $HSeO_3^-$ and SeO_3^{2-} exhibit sorption onto Fe(III) (hydr)oxides and other variably charged mineral surfaces at circumneutral to acidic pH.[21] However, SeO_4^{2-}, the dominant Se(VI) oxyanion at pH > 2, exhibits a relatively weak sorption onto mineral surfaces over a wide pH range.[22] Consequently, Se(IV) is generally less mobile and bioavailable than Se(VI) in the environment. Abiotic or biological reduction of Se(VI) or Se(IV) to insoluble Se(0) can also decrease Se mobility and bioavailability.[5]

Selenium sorption onto Fe(III) (hydr)oxides, including ferrihydrite [$Fe_2O_3{\cdot}9H_2O$], goethite [α-FeOOH], and hematite [Fe_2O_3], has been widely studied.[23−31] More recently, removal by zero-valent iron (ZVI) has been examined as a method for treating Se-contaminated waters.[32−37] These studies examined Se(VI) or Se(IV) removal under both oxic[32,34,35,37] and anoxic[36,38,39] conditions. Previous studies (both oxic and anoxic) generally agree that Se(VI) removal follows three principal steps: (1) Se(VI) reduction to Se(IV) by dissolved or adsorbed Fe(II); (2) Se(IV) sorption onto Fe(III) (hydr)-oxides at ZVI surfaces; and (3) subsequent reduction of Se(IV) to Se(0) or Se(−II) on the ZVI surface.[35−37,40] Additional

Received: November 10, 2016
Accepted: April 4, 2017
Published: April 17, 2017

DOI: 10.1021/acsomega.6b00382
ACS Omega 2017, 2, 1513−1522

research examined different approaches to enhance Se removal, including the introduction of organic matter,[36] transition metals,[38,39] clay minerals,[41,42] and magnetic fields.[43,44] Unfortunately, the Se(VI) concentrations used in previous studies were often considerably higher and did not reflect those typically observed in mine-impacted waters.[34,36] Further, the dominant aqueous concentrations in the tests conducted to determine the influence of ZVI on Se(VI) removal have not represented the chemistry of mine waters.[4,7,12] Mine waters generally contain elevated SO_4^{2-} concentrations derived from sulfide-mineral oxidation[15,16] and elevated NO_3^- concentrations derived from blasting agents commonly used during mining.[17−19] Although these ions have the potential to influence Se(VI) removal by ZVI,[32] their influence on Se(VI) removal rates and mechanisms by ZVI has not been reported. This study examined the influence of SO_4^{2-} and NO_3^- on Se(VI) removal rates and mechanisms by three ZVI materials using environmentally relevant concentrations of SO_4^{2-}, NO_3^-, and Se(VI). Results of this study will inform the development of Se(VI) removal methods for waters impacted by mining and other anthropogenic activities.

RESULTS AND DISCUSSION

Initial ZVI Characteristics. The three unreacted ZVI samples exhibited particle morphologies ranging from angular to subrounded (Figure 1). Reacted ZVI particle morphologies are presented in Figure S1. Surface areas were generally low; however, CGPM exhibited a slightly higher surface area (2.5 m^2 g^{-1}) than both PM and QMP (2.3 m^2 g^{-1}). The minor differences between surface areas of all of the ZVI samples could be attributed to granularity or the presence of oxidation products. These values are in general agreement with previously reported ZVI surface areas of 1.63 m^2 g^{-1} for PM[32] and 0.36 m^2 g^{-1}.[35]

X-ray diffraction (XRD) revealed that all three ZVI materials composed of Fe(0) with magnetite [Fe_3O_4] and minor wüstite [FeO] (Figure S2a). Raman spectra exhibited a strong band for magnetite at ∼670 cm^{-1} (Figure S3a). Two strong bands at ∼1315 and ∼1585 cm^{-1} in all of the three ZVI materials were attributed to the presence of carbon. Overall, the XRD and Raman analyses indicate that ZVI mineralogy was consistent with previous studies.[34,35,46,47]

Se(VI) Removal Rates. The Se(VI) removal was effectively described by first-order reaction kinetics (R^2 = 0.98−0.99), with an additional term (r) included to represent the residual aqueous Se(VI) concentrations (Figure 2, Table 1). Removal of >90% Se(VI) was achieved in 4 h (PM) to 8 h (QMP) in the absence of SO_4^{2-} and NO_3^- (Figure 2a). The removal rates decreased approximately 10 times in the presence of SO_4^{2-} (1800 mg L^{-1}), with 90% Se(VI) removal observed in 50 h (CGPM) to 191 h (QMP) (Figure 2b, Table 1). In contrast, Se(VI) removal rates were decreased 1.5−2.5 times in the presence of NO_3^- ($[NO_3—N]_0$ = 15 mg L^{-1}), with 90% Se(VI) removal observed after 10 h (PM) to 32 h (QMP) (Figure 2c, Table 1). Se(VI) removal rates also decreased in the presence of SO_4^{2-} + NO_3^- (Figure 2d, Table 1), with 90% removal observed after 150 h (PM) to 194 h (CGPM) of reaction time. These rates were similar to those observed for the batches (B2) containing only SO_4^{2-} (Table 1). These results are generally consistent with previous studies on the influence of SO_4^{2-} on Se removal by ZVI. Zhang et al.[32] observed that increasing the SO_4^{2-} concentration from 480 to 48 000 mg L^{-1} decreased the Se removal rate by 65%, that is, from 0.093 to 0.033 h^{-1}. Reinsch et al.[48] reported that both SO_4^{2-} and NO_3^- may promote passivation of ZVI surfaces and therefore a decrease in Se removal efficiency. The fits using first-order reactions were consistent with other studies that used first-order or pseudo-first-order reaction kinetics to describe oxic Se removal by ZVI.[32,34,35,49] Although all of the three ZVI materials exhibited Se(VI) removal capacity, Peerless Metal (PM) was the most effective under the experimental conditions (Table 1). Results indicate that both CGPM and PM are considered to be the more suitable ZVI compared with QMP with respect to the removal rate of Se(VI) from the aqueous solutions tested in this study.

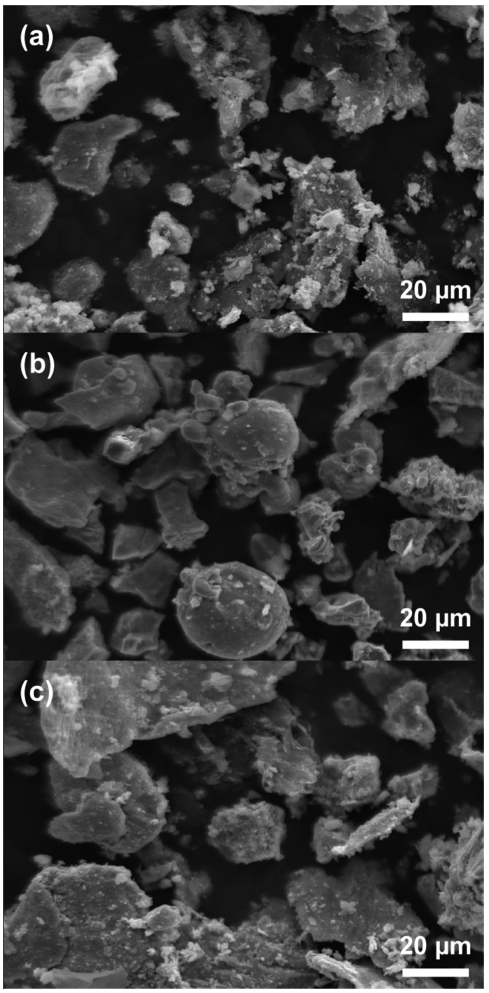

Figure 1. Scanning electron microscopy (SEM) images of unreacted ZVI: (a) CGPM, (b) PM, and (c) QMP. Scale bars are 20 μm.

ZVI Corrosion. Concomitant pH increases and Eh decreases were observed in all batches following ZVI addition (Figure 3). Initial Eh values for all batches ranged from 550 to 575 mV but declined rapidly and stabilized between 200 and 400 mV following ZVI addition. This trend is attributed to the initial ZVI corrosion and subsequent solution equilibration or surface passivation.[46] Initial pH averaged 6.0 ± 0.2 among all batch experiments but rapidly increased to between 7 and 10 following ZVI addition (Figure 3). The largest pH increases were observed in batches containing both SO_4^{2-} and NO_3^- (B4), with pH values for all ZVI materials exceeding 9.0 during the experiment.

Although differences in pH between ZVI materials were observed, the source of these differences was not apparent.

DOI: 10.1021/acsomega.6b00382
ACS Omega 2017, 2, 1513−1522

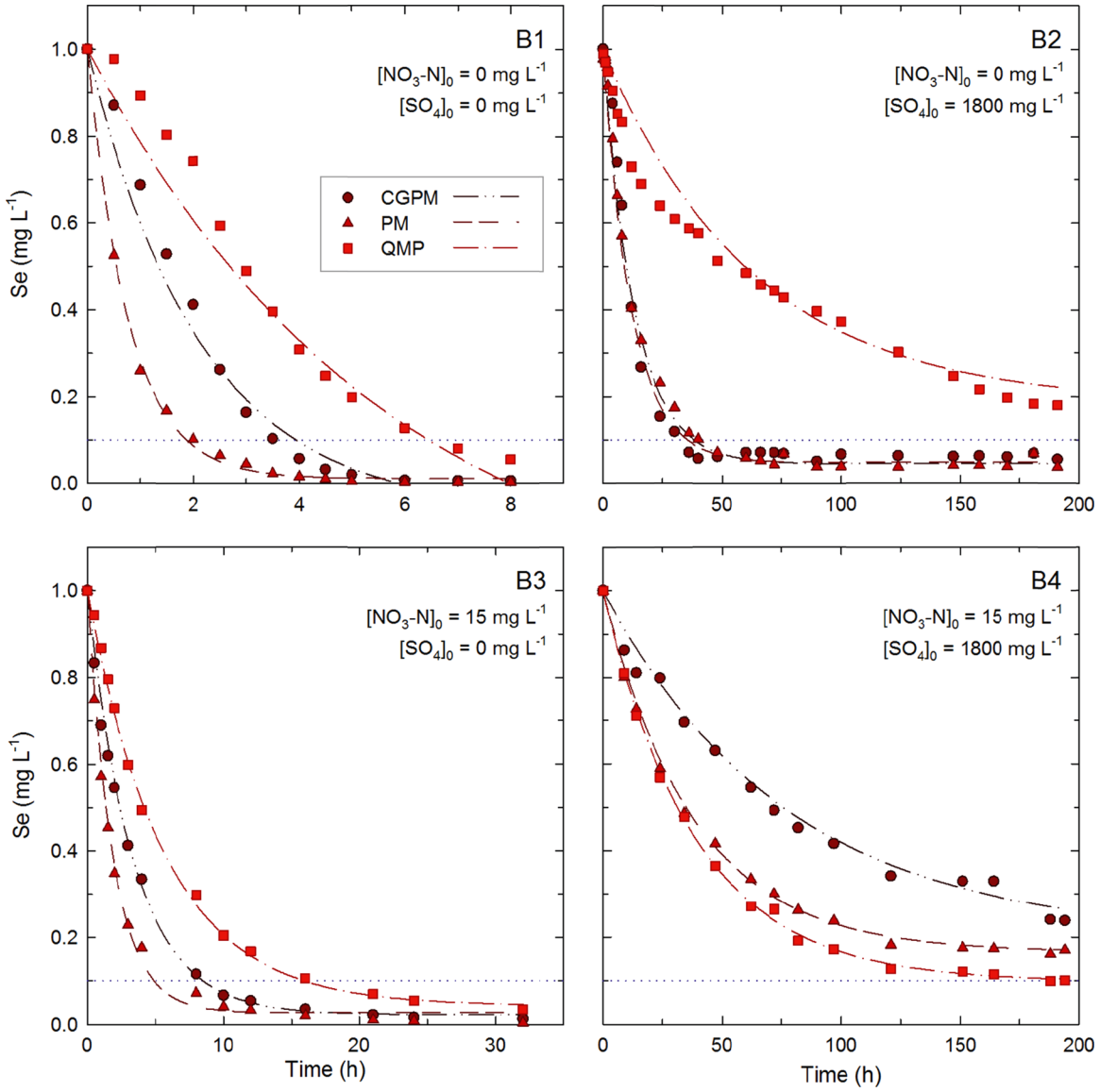

Figure 2. Dissolved Se concentrations with time (data points) and best-fit first-order reaction (lines) for Se removal by ZVI for B1, B2, B3, and B4 batches. The dotted horizontal line represents 90% removal.

Table 1. Modeled First-Order Rate Constants and Fitting Parameters of Se(VI) Removal by ZVI with Time (h) for B1 (1 mg L^{-1} Se), B2 (1 mg L^{-1} Se + 1800 mg L^{-1} SO_4^{2-}), B3 (1 mg L^{-1} Se + 15 mg L^{-1} NO_3—N), and B4 (1 mg L^{-1} Se + 1800 mg L^{-1} SO_4^{2-} + 15 mg L^{-1} NO_3—N)[a]

batch	ZVI	$[A]_0$ (mg L^{-1})	r (mg L^{-1})	k (h^{-1})	R^2
B1	CGPM	1.16 (±0.04)	−0.07 (±0.03)	0.47 (±0.05)	0.98 (±0.05)
	PM	1.08 (±0.01)	0.01 (±0.00)	1.30 (±0.03)	0.99 (±0.01)
	QMP	1.58 (±0.18)	−0.39 (±0.20)	0.18 (±0.04)	0.98 (±0.05)
B2	CGPM	1.22 (±0.03)	0.06 (±0.01)	0.08 (±0.00)	0.99 (±0.04)
	PM	1.16 (±0.01)	0.05 (±0.00)	0.07 (±0.00)	0.99 (±0.02)
	QMP	0.90 (±0.03)	0.20 (±0.03)	0.02 (±0.00)	0.98 (±0.04)
B3	CGPM	0.90 (±0.01)	0.02 (±0.00)	0.30 (±0.01)	0.99 (±0.02)
	PM	1.09 (±0.02)	0.03 (±0.00)	0.53 (±0.02)	0.99 (±0.02)
	QMP	1.08 (±0.01)	0.05 (±0.00)	0.18 (±0.00)	0.99 (±0.02)
B4	CGPM	0.85 (±0.03)	0.21 (±0.03)	0.01 (±0.00)	0.99 (±0.03)
	PM	0.82 (±0.00)	0.16 (±0.00)	0.03 (±0.00)	0.99 (±0.01)
	QMP	0.78 (±0.00)	0.08 (±0.00)	0.03 (±0.00)	0.99 (±0.00)

[a]Initial Se concentration $[A]_0$, residual Se concentrations (r), and rate constant (k), and goodness of fit (R^2) are presented.

DOI: 10.1021/acsomega.6b00382
ACS Omega 2017, 2, 1513−1522

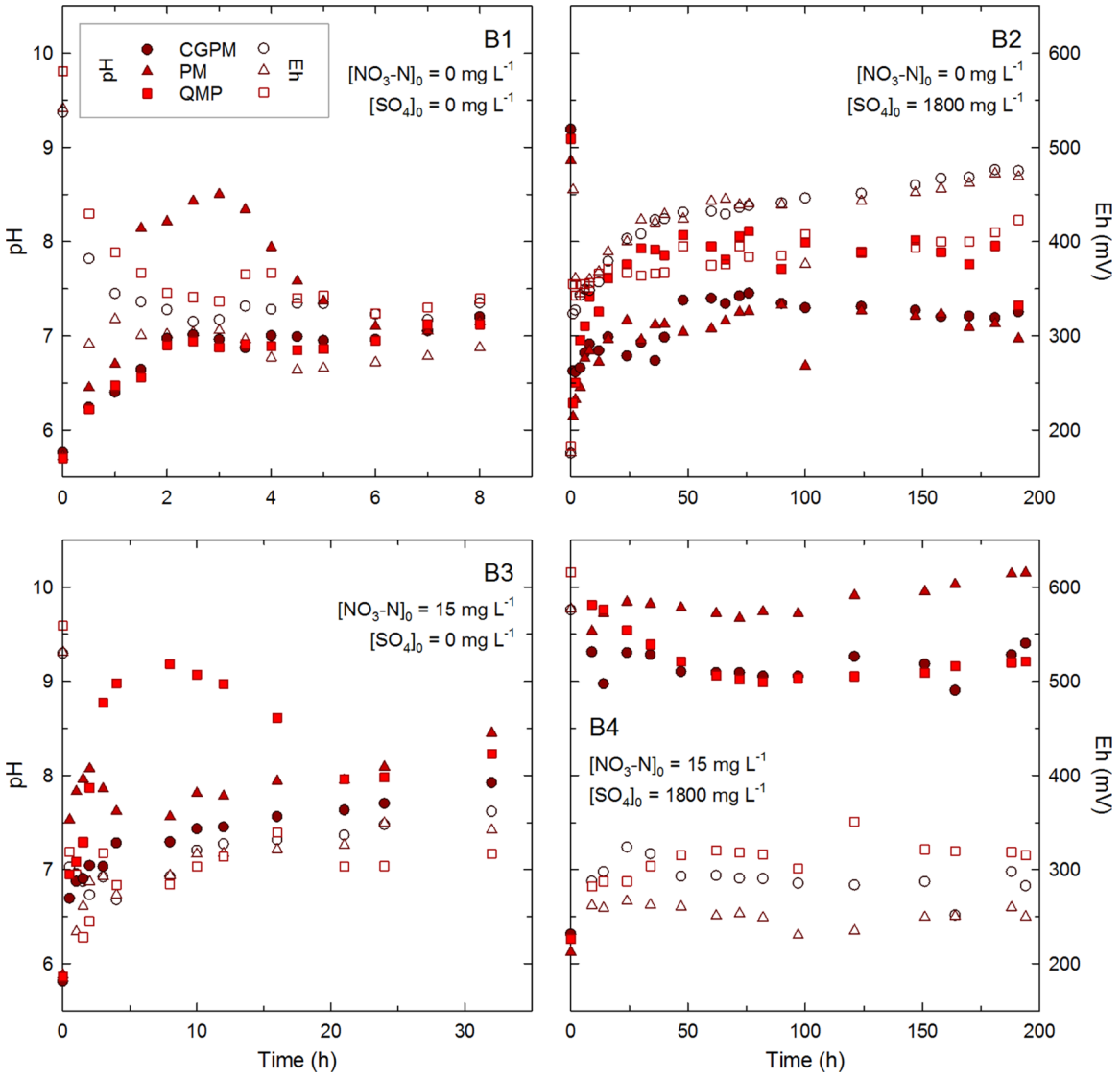

Figure 3. Measured pH and Eh values for B1, B2, B3, and B4 batches.

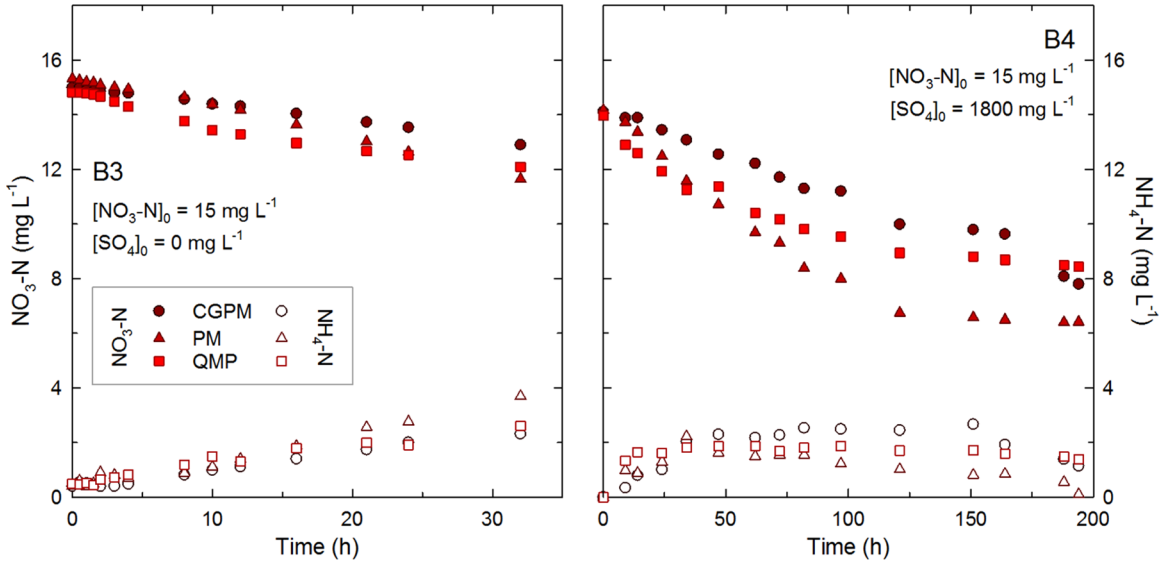

Figure 4. Nitrate (as N) and ammonium (as N) concentrations with time for B3 and B4 batches.

DOI: 10.1021/acsomega.6b00382
ACS Omega 2017, 2, 1513−1522

Subtle differences in the mineralogy of ZVI surface coatings could produce variation in solution pH; however, final pH values for all batches were consistently within 1 pH unit. The increase in pH with reaction time was attributed to ZVI (Fe^0) corrosion, which generates Fe(II), H_2, and OH^-[50]

$$Fe^0 + 2H_2O \rightarrow Fe^{2+} + H_2 + 2OH^- \quad (1)$$

Subsequent $Fe(OH)_{2(s)}$ formation at ZVI surfaces has previously been proposed;[34,50,51] however, this metastable phase forms under anoxic conditions and would rapidly oxidize to Fe(III) (hydr)oxide in the presence of oxygen.[46] Liu et al.[46] proposed an additional ZVI corrosion pathway in the presence of O_2

$$Fe^0 + 1/2O_2 + H_2O \rightarrow Fe^{2+} + 2OH^- \quad (2)$$

Reactions 2 and 3 involve the formation of Fe(II), which would undergo rapid oxidation followed by Fe(III) (hydr)oxide precipitation under oxic conditions at circumneutral pH.[46] Dissolved Fe concentrations were consistently less than 0.02 mg L^{-1} (data not shown), suggesting that the formation of secondary phases controlled the dissolved Fe concentrations in all batches. These observations are generally consistent with previous studies, which reported similar trends to the current study in both Eh and pH during ZVI corrosion.[34,36,46,52]

Nitrate Reduction. In the absence of SO_4^{2-} (B3), NO_3—N concentrations linearly decreased from 15 to 12 mg L^{-1} over 32 h (Figure 4a). Similar results were observed for B4 batches, where NO_3—N concentrations linearly decreased over 34 h from 14 to 11 mg L^{-1} in the presence of SO_4^{2-} (Figure 4b). These data suggest that SO_4^{2-} had a limited influence on NO_3^- reduction by ZVI. Nitrate (NO_3—N) concentrations further decreased in B4 to between 6 and 10 mg L^{-1} after 121 h. Subsequent decreases were limited, and NO_3—N concentrations after 194 h were 7.8 mg L^{-1} (CGPM), 6.4 mg L^{-1} (PM), and 8.4 mg L^{-1} (QMP). These results indicated that ZVI can remove Se(VI) and NO_3^- simultaneously over the pH range of the experiments. These findings are consistent with those of other studies conducted over a wide pH range in the presence and absence of competing ions.[52−55]

Dissolved NH_4^+—N concentrations increased over the first 0.5−32 h in B3 and B4 batches (Figure 4). These increases were generally proportional to decreases in NO_3^-—N concentrations for individual ZVI materials for both batches. However, subsequent decreases in NH_4^+—N concentrations after 50−100 h were observed for B4 batches (Figure 4b).

Desorption measurements suggested that these decreases resulted from NH_4^+—N sorption onto ZVI surfaces with time. More specifically, these measurements revealed that up to 30% of NH_4^+ was adsorbed to reacted ZVI surfaces during the experiments. These findings are consistent with previous studies[52−55] that have reported NH_4^+ formation during NO_3^- reduction by ZVI.

$$4Fe^0 + NO_3^- + 7H_2O = 4Fe^{2+} + NH_4^+ + 10OH^- \quad (3)$$

Nitrate reduction by ZVI has been shown to be a spontaneous process by either an indirect reduction of NO_3^- by hydrogen generated via Fe corrosion (eq 2) or a direct reduction via Fe^0 (eq 3).[52,54]

Secondary Mineralogy. Overall, XRD results show that magnetite and lepidocrocite are the principal products of ZVI reaction under oxic conditions. Distinct magnetite XRD peaks were observed for all ZVI materials after 8 h in the absence of both SO_4^{2-} and NO_3^- (B1). The Fe(0) peaks did show an appreciable increase or decrease in intensity after 8 h (end of the experiment) (Figure S2b). The intensity of the initial wüstite peaks diminished after 8 h, which suggests oxidation had occurred (Figure S2b). Magnetite peaks were observed after 191 h in the presence of SO_4^{2-} (B2). In addition to the magnetite peaks, weak lepidocrocite and goethite peaks developed for ZVI from B2 batches (Figure S2c). The intensity of Fe(0) peaks in B2 diminished considerably compared to those in B1, suggesting more intense oxidation and accompanying ZVI corrosion due to extended reaction time. In contrast to Fe(0), magnetite peaks increased in intensity for the solid samples collected from all B2 batches. This observation suggested that the solid phase from B2 was dominated by magnetite plus minor lepidocrocite, traces of goethite, and residual Fe(0) (Figure S2c). The mineralogies of reacted B3 and B1 samples were generally consistent and composed of Fe(0), magnetite, and wüstite (Figure S2d). Minor lepidocrocite peaks were observed in B3; however, this phase was not detected in reacted B1 solids. These variations may result from the differences in the reaction time (i.e., 8 h for B1 and 32 h for B3) or the role of NO_3^- in ZVI oxidation (Figure S2d). The mineralogies of reacted B4 and B2 ZVI materials were also similar (Figure S2e). For example, B4 and B2 samples were dominated by magnetite and lepidocrocite, plus traces of goethite and residual Fe(0). However, the intensities of the magnetite peaks were lower and those of the lepidocrocite peaks were greater for B2 compared to those of the B4 samples. This observation suggests that although B2 and B4 were reacted for similar time periods (191 h for B2 and 194 h for B4), NO_3^- enhanced ZVI oxidation in B4.

Raman spectral analyses also indicated that magnetite and lepidocrocite were the principal products of ZVI oxidation in all batches. However, Raman spectra exhibited three weak bands at approximately 300, 485, and 548 cm^{-1} because of the presence of goethite phases (Figure S3b−e). Bands for lepidocrocite at approximately 246 and 376 cm^{-1} were stronger for B3 and B4 compared to those for B1 and B2. This observation further suggests that NO_3^- enhances ZVI oxidation (Figure S3d,e). Magnetite bands were better defined for B1 samples (Figure S3b) compared to those for the other three batches (Figure S3c−e), which suggested that reaction time might have contributed to the observed variations in secondary phases. The bands assigned to carbonaceous materials (~1315 and 1585 cm^{-1}) were also visible after aging in all four batches (Figure S3b−e); however, these band intensities were much lower in reacted ZVI samples than in unreacted ZVI samples (Figure S3a).

These XRD and Raman results were supported by SEM analyses (Supporting Information), which also revealed that iron oxides and hydroxides, including magnetite, lepidocrocite, wüstite, and goethite, for during aging of ZVI. The presence of these secondary minerals is consistent with the literature.[34,35,46,56] Although magnetite and lepidocrocite are reported as stable end products of ZVI aging, additional and minor constituents, such as hematite,[57] ferrihydrite,[56] schwertmannite, milkasaite, and vivianite,[48] have also been reported from ZVI aging experiments. These minerals were, however, not observed in the spectral data of the current study.

Solid-Phase Se Speciation. Selenium associated with reacted ZVI solids was dominated by Se(IV) and Se(0) for all batches (Figure 5a−c). Results of linear combination fitting

DOI: 10.1021/acsomega.6b00382
ACS Omega 2017, 2, 1513−1522

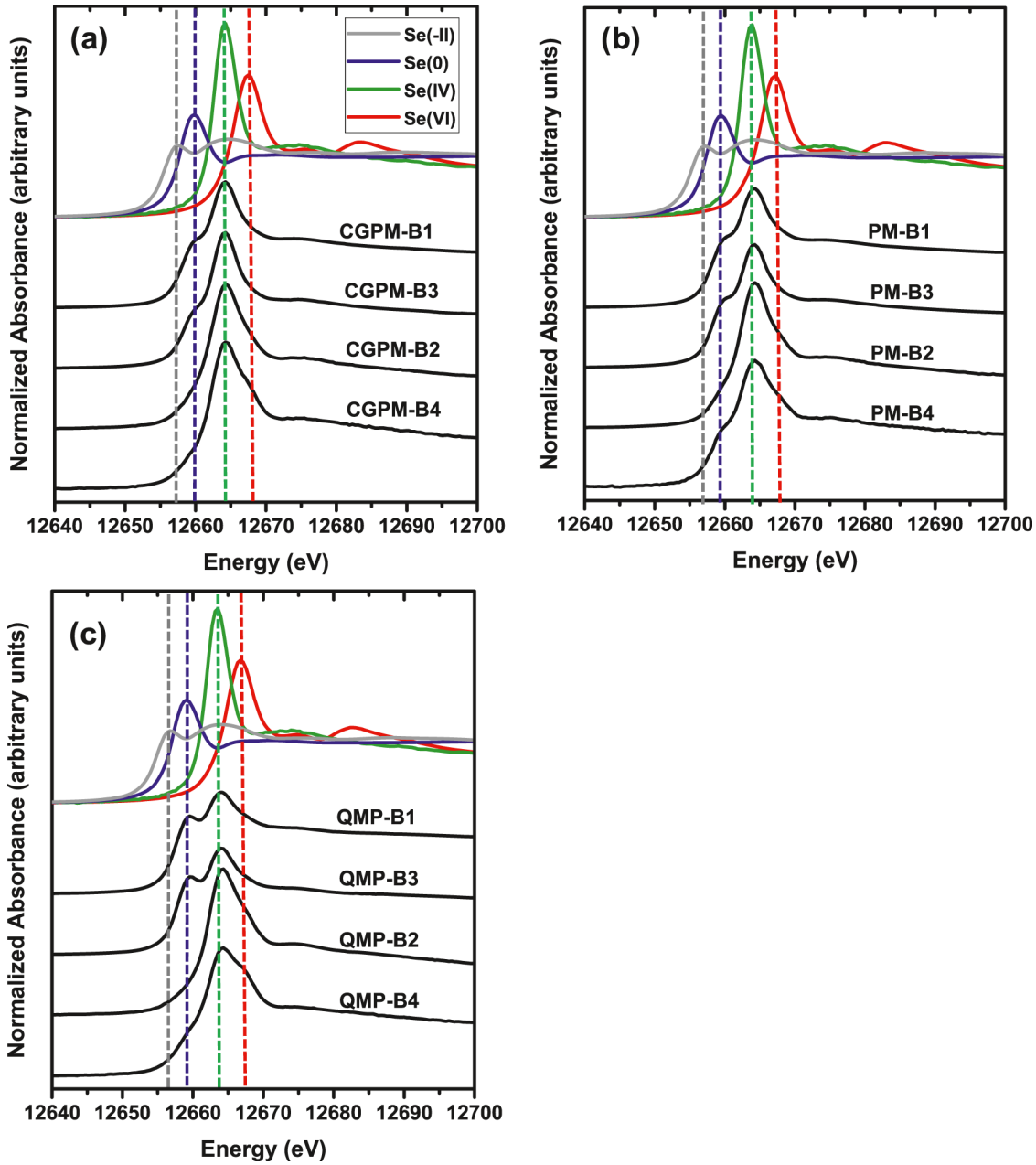

Figure 5. Measured Se K edge XANES spectra of reacted ZVI in (a) CGPM, (b) PM, and (c) QMP forms of reference Se compounds with different oxidation states (selenate, selenite, elemental selenium, and selenide). The dashed vertical lines represent K edge energies for the different oxidation states of Se. The energy values of the first inflection point (E_0) and the white line (most intense peak) for the reference standards are presented in Table S1.

(LCF) analyses indicate that Se(IV) and Se(0) account for >95% of Se on reacted ZVI from B1 and B3 samples. This observation suggests that ZVI effectively reduces Se(VI) to Se(IV) and Se(0) in the absence of sulfate. However, using the LCF Se(0) content as a measure of the reduction extent, the results (Table 2) indicate that Se reduction in both B1 and B3 was the lowest in the CGPM samples (mean Se(0) = 45%) and the highest in the QMP samples (mean Se(0) = 64.4%).

This finding is illustrated by B3 LCF results (Figure S4), which exhibit Se(0) content following the general order QMP > PM > CGPM. The mean Se(0) content of B1 samples (55%) was also slightly greater than that of B3 samples (52%), perhaps suggesting that NO_3^- inhibits Se(VI) reduction by ZVI. Se(IV) was the predominant oxidation state in B2 (mean = 66%) and B4 (mean = 57%) samples (Table 2), whereas Se(0) accounted for 23% (B2) and 32% (B3). Additionally, the mean Se(VI) content for B2 (17%) and B4 (17%) is substantially greater than that for B1 (4%) and B3 (4%) samples. These results indicate that SO_4^{2-}, present at 1800 mg L^{-1} in B2 and B4 batches, limited Se(VI) reduction to Se(0) by ZVI. However, the extent of Se(VI) reduction to Se(0) was slightly greater in B4 samples (mean Se(0) = 32%) compared to that in B2 samples (mean Se(0) = 22.6%). This observation suggests that NO_3^- somewhat diminishes the limiting effect of SO_4^{2-} on Se reduction by ZVI. The proportions of Se(IV) and Se(0) were similar for CGPM and PM; however, Se(0) was the dominant oxidation state for QMP.

DOI: 10.1021/acsomega.6b00382
ACS Omega 2017, 2, 1513−1522

Table 2. Linear Combination Fitting of Se K Edge XANES Spectra for Reacted ZVI from B1 (1 mg L^{-1} Se), B2 (1 mg L^{-1} Se + 1800 mg L^{-1} SO_4^{2-}), B3 (1 mg L^{-1} Se + 15 mg L^{-1} NO_3—N), and B4 (1 mg L^{-1} Se + 1800 mg L^{-1} SO_4^{2-} + 15 mg L^{-1} NO_3—N)

batch	ZVI	Se(VI)	Se(IV)	Se(0)	Se(−II)	total	*R*-factor
B1	CGPM	4.8 (±0.8)	50.7 (±0.8)	50.1 (±2.0)		105.6	0.004
	PM	4.8 (±0.8)	46.9 (±0.8)	52.3 (±2.1)		104.1	0.005
	QMP	2.6 (±0.8)	31.5 (±0.7)	63.4 (±1.9)	5.9 (±2.2)	103.4	0.005
B2	CGPM	15.7 (±1.0)	65.8 (±1.0)	24.3 (±2.5)		105.8	0.009
	PM	14.1 (±1.0)	66.7 (±0.9)	25.0 (±2.5)		105.9	0.008
	QMP	21.1 (±1.1)	66.4 (±1.0)	18.6 (±2.6)		106.2	0.009
B3	CGPM	5.0 (±0.8)	58.8 (±0.8)	40.0 (±2.0)		103.8	0.004
	PM	4.7 (±0.8)	49.7 (±0.8)	49.7 (±2.1)		104.1	0.005
	QMP	2.6 (±0.7)	35.6 (±0.7)	65.4 (±1.7)		103.6	0.004
B4	CGPM	18.8 (±1.2)	66.7 (±1.1)	21.9 (±2.9)		107.4	0.012
	PM	11.7 (±1.1)	52.9 (±1.1)	42.6 (±2.5)		107.1	0.010
	QMP	21.2 (±1.1)	52.8 (±1.1)	32.2 (±2.8)		106.3	0.011

The LCF results for B1, B2, B3, and B4 samples suggest the presence of other oxyanions, such as NO_3^- and SO_4^{2-}, with Se(VI) in solution limiting the rate and extent of Se(VI) reduction by ZVI. The observed order of the extent Se reduction in the samples tested is B1 > B3 > B4 > B2. The results of the analysis also indicate that the type of ZVI also affects the extent of Se reduction associated with Se(VI) removal. Generally, the observed order of Se(VI) reduction to either Se(IV) or Se(0) from solution by the source of the ZVI is CGPM < PM < QMP. These results are consistent with the modeled Se(VI) removal rates (Table 1, Figure 2), which revealed that Se(VI) removal was most effective for CGPM and PM than for QMP. Nevertheless, Se(VI) removal rates in the presence of both NO_3^- and SO_4^{2-} (i.e., B4) were slightly greater for QMP and PM than for CGPM.

The XANES results are consistent with limited published results in the literature, where reduced Se species (i.e., Se(IV), Se(0), and Se(−II)) are formed during Se(VI) removal by ZVI.[34,35,58] The results of this study indicate that Se(VI) removal involves the reduction of dissolved Se(VI) to predominantly Se(IV) and Se(0), which are associated with ZVI surfaces. The results also show that Se(VI) reduction and removal proceeded in the presence of other oxyanions (i.e., NO_3^- and SO_4^{2-}).

CONCLUSIONS

Contamination of surface waters and groundwater by Se(VI) is a global problem often associated with anthropogenic activities, including mining and mineral processing. There is a pressing need to develop cost-effective techniques for treating these waters. Sorption onto Fe oxides and hydroxides is an important Se(VI) attenuation mechanism in the environment.[24,28,31] Adsorption capacity is surface-area-controlled, and Se(VI) removal via this mechanism may, therefore, be limited. Recent studies have demonstrated that ZVI can promote Se(VI) removal via adsorption and reduction to low-solubility Se species.[32,34,35,38,39] Unlike adsorption on iron oxides and hydroxides, the capacity for Se(VI) removal by adsorption and reduction using ZVI is substantially increased.[59] However, the impact of competing ions on Se(VI) removal by ZVI from mining-impacted waters, which commonly contain high SO_4^{2-} and NO_3^- concentrations, remains uncertain.

This study evaluated Se(VI) removal rates and mechanisms for three commercial ZVI materials under oxic and near-neutral pH conditions and in the presence of SO_4^{2-} and NO_3^-. Batch experiments revealed rapid Se(VI) removal in the absence of both SO_4^{2-} and NO_3^-. Although Se(VI) removal rates decreased substantially in the presence of NO_3^- and SO_4^{2-}, >99% removal was achieved over longer times. The Se(VI) removal process for all batches was described by first-order reaction kinetics with the inclusion of a residual Se(VI) component. In addition to Se(VI) removal, all of the three ZVI exhibited the ability to partially remove NO_3^- via reduction and/or sorption mechanisms. Solid-phase analyses revealed that Fe(0) oxidizes to magnetite, lepidocrocite, wüstite, and goethite with time. Furthermore, XANES analyses showed that Se(VI) was reduced to a mixture of Se(IV) and Se(0) associated with ZVI solids. This study suggests that ZVI can effectively remove Se(VI) from mining-impacted waters, which commonly contain elevated SO_4^{2-} and NO_3^- concentrations.

MATERIALS AND METHODS

Zero-Valent Iron. Selenium(VI) removal rates and mechanisms were examined using three commercially available ZVI materials: (1) ground-cast Fe aggregate (ETI CC-1004; 0.368−2.36 mm) from Connelly-GPM Inc. (CGPM; Chicago, IL); (2) ground-cast Fe aggregate (8/50; 0.368−2.36 mm) from Peerless Metal Powder and Abrasives (Detroit, MI); and (3) metallurgical granular Fe (H_2Omet 58; 0.075−1.68 mm) from Rio Tinto Metal Powders (QMP; Montreal, Canada). These ZVI materials contained >90% Fe with minor to trace impurities, including C, O, S, Mn, V, Cu, and Cr (quantified by the suppliers). The ZVI materials were used as received from the suppliers; surface coatings were not removed before initiating the experiments.

Batch Experiments. Four batch experiments were conducted to assess Se(VI) removal using all of the three ZVI materials. These experiments included: (B1) Se(VI); (B2) Se(VI) + SO_4^{2-}; (B3) Se(VI) + NO_3^-; and (B4) Se(VI) + SO_4^{2-} + NO_3^-. Solutions were prepared by dissolving $NaSeO_4$ (0.0024 g) in 1 L of Type-1 ultrapure water (i.e., 18.2 MΩ cm) and adding Na_2SO_4 (3.24 g) and $NaNO_3$ (0.0753 g). These masses produced Se(VI), SO_4^{2-}, and NO_3—N concentrations of 1, 1800, and 15 mg L^{-1}, respectively, which are consistent with drainage from coal spoils.[4,12] The solutions were prepared in 2 L polyethylene (PE) beakers and continuously stirred at 300 rpm under ambient conditions (i.e., ∼22 °C, atmospheric O_2) throughout the experiment. The experiment was initiated by adding 10 g of ZVI to each solution such that Se(VI) removal by each material (CGPM, PM, and QMP) was evaluated for each solution (B1, B2, B3, and B4).

DOI: 10.1021/acsomega.6b00382
ACS Omega 2017, 2, 1513−1522

Water Sampling and Analysis. Water sampling and geochemical measurements were performed before initiating the experiment and subsequently at time intervals of 30 min to 30 h for up to 200 h. Measurements of pH and redox potential (Eh) were performed in conjunction with water sampling. The pH electrode (VWR Symphony) was calibrated to NIST-traceable 4, 7, and 10 buffer solutions. The electrode performance was regularly checked, and recalibration was performed as necessary. The performance of the redox electrode (Accumet) was verified using ORP calibration solution (Orion). The water samples were collected in PE syringes, passed through 0.2 μm polyethersulfone (PES) syringe filter membranes, stored in high-density PE (HDPE) bottles, and refrigerated until analysis. Inorganic anions (NO_3^-, NO_2^-, and SO_4^{2-}) were quantified by ion chromatography (ICS2100; Dionex Corporation) on nonacidified samples. Total Se was quantified by inductively coupled plasma−optical emission spectroscopy (SPECTROBLUE SOP, SPECTRO Analytical Instruments GmbH, Germany) on samples acidified to pH < 2 with trace-metal-grade nitric acid (Thermo Fisher Scientific). Spectrophotometric (DR2800; HACH Chemical Co.) determination of total ammonium (NH_4^+) concentrations (by the Nessler method) was performed for samples from B3 and B4, which initially contained NO_3^-.

Solid-Phase Sampling and Analyses. Samples of the three reacted ZVI materials (i.e., CGPM, PM, and QMP) from each batch (i.e., B1, B2, B3, and B4) were collected at the end of the experiment. These samples were freeze-dried and refrigerated until analysis (up to 30 days). XRD, Raman spectroscopy (RS), SEM, and Brunauer−Emmett−Teller (BET) surface-area analyses were used to examine the physical, chemical, and mineralogical characteristics of the three initial ZVI materials (n = 3) and the reacted ZVI samples (n = 12). These samples were gently ground in an agate mortar and pestle before analysis. Samples from each of the B1 batches were analyzed to assess the reproducibility of the results. X-ray absorption near-edge structure (XANES) spectroscopy was performed on the reacted ZVI samples (n = 12) to examine Se speciation in the reaction products.

XRD. Samples were mounted on glass plates, which were then placed on a spinning reflection/transmission stage of an X-ray diffractometer (Empyrean, PANalytical B.V., the Netherlands). The power supply and Co X-ray tube were operated at 40 kV and 45 mA, respectively. An incident beam path Fe Kβ-filter, 1° antiscatter slit, 0.02 mm Soller slits, and divergence and receiving slits each fixed at 0.5° and spectral acquisitions were used during data acquisition. Diffraction patterns were obtained from 10 to 80° with a step size of 0.0167° and a scan speed of 1° min^{-1}. Phase identification was performed using search-match software (HighScore Plus, PANalytical B.V., the Netherlands) and the ICDD database (International Center for Diffraction Data).

RS. The Raman microscope (inVia Reflex, Renishaw plc, U.K.) was equipped with a solid-state laser diode operated at 785 nm and 1200 lines mm^{-1} grating. Following wavenumber calibration using an internal silicon standard (Raman shift, 520 cm^{-1}), a few milligrams of each sample were placed on a glass slide and viewed under a 20× N PLAN microscope objective with 0.40 numerical aperture (Leica Microsystems GmbH, Germany). Backscattered Raman signals were collected (32 spectral accumulations) with a Peltier-cooled charge-coupled device detector, operated in the line focus confocal mode with a 10 s detector exposure and 0.1% laser power.

SEM. Samples were mounted onto 10 mm aluminum pin stub mounts using double-sided carbon tape. A 200 Å thick gold coating was then applied using a plasma sputter coater (S150B; Edwards High Vacuum, U.K.). Scanning electron images were obtained using an SEM (JSM-840A; JEOL Ltd., Japan) with digital image acquisition system (dPict7, Micro-Ånalytical Laboratory Inc.). The SEM was operated using a 20 kV acceleration voltage at 1500× magnification and a 25 mm working distance.

Surface Area. The surface area was quantified by obtaining 11-point BET-nitrogen isotherms (NOVA 2200e, Quantachrome Instruments). The multipoint BET surface area of each sample was measured at atmospheric pressure, and the adsorption isotherms achieved a p/p_0 range of 0.05−0.35. Samples were degassed at 70 °C for 24 h before analysis.

X-ray Absorption Spectroscopy. Selenium K edge XAS spectra were collected at the Hard X-ray Micro-Analysis beamline (HXMA-06ID-1) at the Canadian Light Source (Saskatoon, Canada). The beamline utilizes a 2 T superconducting wiggler with rhenium-coated mirrors for upstream collimating and downstream beam focusing. Paired Si(111) crystals were used to monochromatize the incident white beam. Higher harmonics were rejected by detuning the second monochromator to 50% of the fully tuned beam intensity. The monochromator step size was reduced to 0.25 eV in the XANES region, and constant 0.05 $Å^{-1}$ steps in k-space were used in the extended X-ray absorption fine structure (EXAFS) region to 9.2k.

Samples and reference materials were ground in an agate mortar and pestle before being loaded into 0.5 mm thick poly(tetrafluoroethylene) sample holders and sealed between two layers of polyimide tape. References materials included Se(VI) ($NaSeO_{4(s)}$) Se(IV) sorbed onto ferrihydrite, Se(0) ($Se_{(s)}$), and Se(−II) ($FeSe_{(s)}$). The Se(VI), Se(0), and Se(−II) reference materials were diluted with boron nitride. Sample spectra were collected under ambient conditions in fluorescence mode using a 32-element solid-state Ge detector (Canberra Industries Inc.). Aluminum foil, a Soller slit, and an arsenic filter were placed between the sample and the detector to reduce scattering and Fe fluorescence, which, therefore, enhance the Se fluorescence signal. Reference spectra were collected in transmission mode under ambient conditions between the first and second ionization chamber detectors. Transmission spectra for Se foil positioned between the second and third ionization chambers were used for energy calibration during data reduction. Four spectra were collected and averaged for all samples, whereas duplicate scans were collected and averaged for each reference material.

The ATHENA module of the Demeter (v.0.9.24) XAS software package[45] was used for data reduction and XANES analyses. Individual Se K edge XAS scans were calibrated to the second derivative zero crossing of the reference Se foil. Following calibration, replicate scans were averaged to improve signal-to-noise ratios. Background removal and normalization were subsequently performed on averaged spectra. The relative percentages of Se redox species were assessed for normalized XANES spectra using LCF over the energy range of 12 640−12 690 eV, assuming that this is representative of the sample as a whole. The residual factors (R) of the best fits provided a measure of the goodness of fit, with smaller values indicating a better fit. The total values also reflected the goodness of fit as the totals are not constrained in the fits, and, as such, better fits are represented by the totals closest to 100.

DOI: 10.1021/acsomega.6b00382
ACS Omega 2017, 2, 1513−1522

Ammonium Desorption. Ammonium (NH_4^+) adsorbed onto ZVI during Se removal in B4 batches was quantified following desorption at acidic pH. Approximately 0.5 g of reacted ZVI was combined with 119.5 mL of Type-1 ultrapure water in a 200 mL PE beaker to achieve a final volume of 120 mL. The solution was stirred at 100 rpm for 5 min, and the pH was adjusted to 1 using 1 M HCl. Following 24 h of continuous stirring, 1 mL of solution was passed through a 0.2 μm PES syringe filter, and NH_4^+ was quantified by spectrophotometry as previously described.

Modeling Selenium Removal Kinetics. Best-fit first-order reaction rates for Se removal were determined using

$$[A]_t = [A]_0 \, e^{-kt} + r \quad (4)$$

where $[A]_t$ is the Se concentration (mg L^{-1}) at time t (h), $[A]_0$ is the initial Se concentration (mg L^{-1}), k is the rate constant (h^{-1}), t is time (h), and r is the residual aqueous Se concentration (mg L^{-1}). The R^2 values for the best fits are indicative of the goodness of fits, where values closer to 1 indicate a better fit.

■ ASSOCIATED CONTENT

Supporting Information

The Supporting Information is available free of charge on the ACS Publications website at DOI: 10.1021/acsomega.6b00382.

Detailed XRD, Raman, SEM analyses of reacted and unreacted ZVI (four figures and one table).

■ AUTHOR INFORMATION

Corresponding Author

*E-mail: sod671@campus.usask.ca. Tel: 306-966-4664. Fax: 306-966-8593.

ORCID

Soumya Das: 0000-0003-1848-0164

Matthew B. J. Lindsay: 0000-0001-9123-3261

Notes

The authors declare no competing financial interest.

■ ACKNOWLEDGMENTS

Funding was provided by the Natural Sciences and Engineering Research Council of Canada (NSERC) IRC program (M.J.H.; Grant No. 184573), Discovery Grants program (M.B.J.L.; Grant No. RGPIN-2014-06589), and Cameco Corporation (M.J.H.). The Canadian Light Source is supported by the Canada Foundation for Innovation, NSERC, the University of Saskatchewan, the Government of Saskatchewan, Western Economic Diversification Canada, the National Research Council Canada, and the Canadian Institutes of Health Research.

■ REFERENCES

(1) Lemly, A. D. Aquatic selenium pollution is a global environmental safety issue. *Ecotoxicol. Environ. Saf.* **2004**, *59*, 44−56.

(2) Muscatello, J. R.; Janz, D. M. Selenium accumulation in aquatic biota downstream of a uranium mining and milling operation. *Sci. Total Environ.* **2009**, *407*, 1318−1325.

(3) Griffith, M. B.; Norton, S. B.; Alexander, L. C.; Pollard, A. I.; LeDuc, S. D. The effects of mountaintop mines and valley fills on the physicochemical quality of stream ecosystems in the central Appalachians: A review. *Sci. Total Environ.* **2012**, *417*−*418*, 1−12.

(4) Wellen, C. C.; Shatilla, N. J.; Carey, S. K. Regional scale selenium loading associated with surface coal mining, Elk Valley, British Columbia, Canada. *Sci. Total Environ.* **2015**, *532*, 791−802.

(5) Fordyce, F. Selenium geochemistry and health. *Ambio* **2007**, *36*, 94−97.

(6) Leybourne, M. I.; Cameron, E. M. Source, transport, and fate of rhenium, selenium, molybdenum, arsenic, and copper in groundwater associated with porphyry−Cu deposits, Atacama Desert, Chile. *Chem. Geol.* **2008**, *247*, 208−228.

(7) Lussier, C.; Veiga, V.; Baldwin, S. The geochemistry of selenium associated with coal waste in the Elk River Valley, Canada. *Environ. Geol.* **2003**, *44*, 905−913.

(8) WHO. Selenium in Drinking-Water. Background Document for Development of WHO Guidelines for Drinking-Water Quality, Geneva, Switzerland, 2011.

(9) Water and Air Quality Bureau. Healthy Environments and Consumer Safety Branch, Health Canada. Guidelines for Canadian Drinking Water Quality Summary Table; Water and Air Quality Bureau, Healthy Environments and Consumer Safety Branch, Health Canada: Ottawa, Ontario, Canada, 2014.

(10) Office of Water, United States Environmental Protection Agency (U.S. EPA). Drinking Water Standards and Health Advisories; Office of Water, U.S. EPA: Washington, DC, EPA 822-R-06-013, 2006.

(11) CCME. Canadian Soil Quality Guideline for Selenium: Environmental and Human Health Effects, 2009.

(12) Hendry, M. J.; Biswas, A.; Essilfie-Dughan, J.; Chen, N.; Day, S. J.; Barbour, S. L. Reservoirs of selenium in coal waste rock: Elk Valley, British Columbia, Canada. *Environ. Sci. Technol.* **2015**, *49*, 8228−8236.

(13) Diehl, S. F.; Goldhaber, M.; Koenig, A. E.; Lowers, H. A.; Ruppert, L. Distribution of arsenic, selenium, and other trace elements in high pyrite Appalachian coals: evidence for multiple episodes of pyrite formation. *Int. J. Coal Geol.* **2012**, *94*, 238−249.

(14) Kolker, A. Minor element distribution in iron disulfides in coal: A geochemical review. *Int. J. Coal Geol.* **2012**, *94*, 32−43.

(15) Lindsay, M. B. J.; Moncur, M. C.; Bain, J. G.; Jambor, J. L.; Ptacek, C. J.; Blowes, D. W. Geochemical and mineralogical aspects of sulfide mine tailings. *Appl. Geochem.* **2015**, *57*, 157−177.

(16) Essilfie-Dughan, J.; Hendry, M. J.; Dynes, J.; Hu, Y.; Biswas, A.; Lee Barbour, S.; Day, S. Geochemical and Mineralogical Characterization of Sulfur and Iron in Coal Waste Rock, Elk Valley, British Columbia, Canada. *Sci. Total Environ.* **2017**, *586*, 753.

(17) Bailey, R. T.; Gates, T. K.; Halvorson, A. D. Simulating variably-saturated reactive transport of selenium and nitrogen in agricultural groundwater systems. *J. Contam. Hydrol.* **2013**, *149*, 27−45.

(18) Szmigielski, J. T. Characterizing a Groundwater System Downgradient of a Coal Mine Waste Rock Dump, Elk Valley, British Columbia, Canada. M.Sc. Thesis, University of Saskatchewan, 2015.

(19) Mahmood, F. N.; Barbour, S. L.; Hendry, M. J.; Kennedy, C. Nirate release from a coal waste rock dump, submitted for publication, 2017.

(20) Kabata-Pendias, A. Geochemistry of selenium. *J. Environ. Pathol., Toxicol. Oncol.* **1998**, *17*, 173−177.

(21) Balistrieri, L. S.; Chao, T. T. Adsorption of selenium by amorphous iron oxyhydroxide and manganese dioxide. *Geochim. Cosmochim. Acta* **1990**, *54*, 739−751.

(22) Hayes, K. F.; Roe, A. L.; Brown, G. E., Jr.; Hodgson, K. O.; Leckie, J. O.; Parks, G. A. In situ x-ray absorption study of surface complexes: selenium oxyanions on α-FeOOH. *Science* **1987**, *238*, 783−786.

(23) Balistrieri, L. S.; Chao, T. T. Selenium adsorption by goethite. *Soil Sci. Soc. Am. J.* **1987**, *51*, 1145−1151.

(24) Manceau, A.; Charlet, L. The mechanism of selenite adsorption on goethite and hydrous ferric oxide. *J. Colloid Interface Sci.* **1994**, *168*, 87−93.

(25) Su, C.; Suarez, D. L. Selenate and selenite sorption on iron oxides: an infrared and electrophoretic study. *Soil Sci. Soc. Am. J.* **2000**, *64*, 101−111.

DOI: 10.1021/acsomega.6b00382
ACS Omega 2017, 2, 1513−1522

(26) Rietra, R. P. J. J.; Hiemstra, T.; van Riemsdijk, W. H. Comparison of selenite and sulfate adsorption on goethite. *J. Colloid Interface Sci.* **2001**, *240*, 384−390.
(27) Kang, Y.; Inoue, N.; Rashid, M. M.; Sakurai, K. Fixation of soluble selenium in contaminated soil by amorphous iron (hydr)oxide. *Environ. Sci.* **2002**, *15*, 173−182.
(28) Peak, D.; Sparks, D. L. Mechanism of selenite adsorption on iron oxides and hydroxides. *Environ. Sci. Technol.* **2002**, *36*, 1460−1466.
(29) Rovira, M.; Giménez, J.; Martínez, M.; Martínez-Llado, X.; de Pablo, J.; Martí, V.; Duro, L. Sorption of selenium(IV) and selenium(VI) onto natural iron oxides: goethite and hematite. *J. Hazard. Mater.* **2008**, *150*, 279−284.
(30) Chan, Y. T.; Kuan, W. H.; Chen, T. Y.; Wang, M. K. Adsorption mechanism of selenite and selenite on the binary oxide systems. *Water Res.* **2009**, *43*, 4412−4420.
(31) Das, S.; Hendry, M. J.; Essilfie-Dughan, J. Adsorption of selenite onto ferrihydrite, goethite, and lepidocrocite under neutral pH conditions. *Appl. Geochem.* **2013**, *28*, 185−193.
(32) Zhang, Y.; Wang, J.; Amrhein, C.; Frankenberger, W. T., Jr. Removal of selenate from water by zerovalent iron. *J. Environ. Qual.* **2005**, *34*, 487−495.
(33) McCloskey, J.; Twidwell, L.; Park, B.; Fallon, M. In *Removal of Selenium Oxyanions from Industrial Scrubber Waters Utilizing Elemental Iron*, Proceedings of the Sixth International Symposium Hydrometallurgy, 2008; pp 140−148.
(34) Olegario, J. T.; Yee, N.; Miller, M.; et al. Reduction of Se(VI) to Se(-II) by zerovalent iron nanoparticle suspensions. *J. Nanopart. Res.* **2010**, *12*, 2057−2068.
(35) Yoon, I.-H.; Kim, K.-W.; Bang, S.; Kim, M. G. Reduction and adsorption mechanisms of selenite by zero-valent iron and related corrosion. *Appl. Catal., B* **2011**, *104*, 185−192.
(36) Gibson, B. D.; Blowes, D. W.; Lindsay, M. B. J.; Ptacek, C. J. Mechanistic investigations of Se(VI) treatment in anoxic groundwater using granular iron and organic carbon. *J. Hazard. Mater.* **2012**, *241−242*, 92−100.
(37) Liang, L.; Yang, W.; Guan, X.; Li, J.; Xu, Z.; Wu, J.; Huang, Y.; Zhang, X. Kinetics and mechanisms of pH-dependent selenite removal by zero valent iron. *Water Res.* **2013**, *47*, 5846−5855.
(38) Tang, C.; Huang, Y. H.; Zeng, H.; Zhang, Z. Reductive removal of selenate by zero-valent iron: the roles of aqueous Fe^{2+} and corrosion products, and selenate removal mechanism. *Water Res.* **2014**, *67*, 166−174.
(39) Tang, C.; Huang, Y. H.; Zeng, H.; Zhang, Z. Promotion effect Mn^{2+} and Co^{2+} on selenate reduction by zero-valent iron. *Chem. Eng. J.* **2014**, *244*, 97−104.
(40) Yoon, I.-H.; Bang, S.; Kim, K.-W.; Kim, M. G.; Park, S. Y.; Choi, W.-K. Selenate removal by zero-valent iron in oxic condition: the role of Fe(II) and selenate removal mechanism. *Environ. Sci. Pollut. Res.* **2016**, *23*, 1081−1090.
(41) Li, Y.; Cheng, W.; Sheng, G.; Li, J.; Dong, H.; et al. Synergetic effect of a pillared bentonite support on SE(VI) removal by nanoscale zero valent iron. *Appl. Catal., B* **2015**, *174−175*, 329−335.
(42) Dong, H.; Chen, Y.; Sheng, G.; Li, J.; Cao, J.; Li, Z.; Li, Y. The roles of a pillared bentonite on enhancing Se(VI) removal by ZVI and the influence of co-existing solutes in groundwater. *J. Hazard. Mater.* **2016**, *304*, 306−312.
(43) Liang, L.; Guan, X.; Shi, Z.; Li, J.; Wu, Y.; Tratnyek, P. G. Coupled effects of aging and weak magnetic fields on sequestration of selenite by zero-valent iron. *Environ. Sci. Technol.* **2014**, *48*, 6326−6334.
(44) Liang, L.; Sun, W.; Guan, X.; Huang, Y.; Choi, W.; Bao, H.; Li, J.; Jiang, Z. Weak magnetic field significantly enhances selenite removal kinetics by zero valent iron. *Water Res.* **2014**, *49*, 371−380.
(45) Ravel, B.; Newville, M. ATHENA, ARTEMIS, HEPHAESTUS: data analysis for X-ray absorption spectroscopy using IFEFFIT. *J. Synchrotron Radiat.* **2005**, *12*, 537−541.
(46) Liu, A.; Liu, J.; Han, J.; Zhang, W.-X. Evolution of nanoscale zero-valent iron (nZVI) in water: microscopic and spectroscopic evidence on the formation of nano- and micro-structured iron oxides. *J. Hazard. Mater.* **2017**, *322*, 129.
(47) Firdous, R. Factors Affecting Reactivity of Granular Iron in Contact with Chlorinated Solvents. Ph.D. Dissertation, University of Kansas, 2013; p 251.
(48) Reinsch, B. C.; Forsberg, B.; Penn, R. L.; Kim, C. S.; Lowry, G. V. Chemical transformations during aging of zerovalent iron nanoparticles in the presence of common groundwater dissolved constituents. *Environ. Sci. Technol.* **2010**, *44*, 3455−3461.
(49) Shrimpton, H. K.; Blowes, D. W.; Ptacek, C. J. Fractionation of selenium during selenite reduction by granular zerovalent iron. *Environ. Sci. Technol.* **2015**, *49*, 11688−11696.
(50) Manning, B. A.; Hunt, M. L.; Amrhein, C.; Yarmoff, J. A. Arsenic(III) and arsenic(V) reactions with zerovalent iron corrosion products. *Environ. Sci. Technol.* **2002**, *36*, 5455−5465.
(51) Farrell, J.; Wang, J.; O'Day, P.; Conklin, M. Electrochemical and spectroscopic study of arsenate removal from water using zero-valent iron media. *Environ. Sci. Technol.* **2001**, *35*, 2026−2032.
(52) Su, C.; Puls, R. W. Nitrate reduction by zerovalent iron: effects of formate, oxalate, citrate, chloride, sulfate, borate, and phosphate. *Environ. Sci. Technol.* **2004**, *38*, 2715−2720.
(53) Suzuki, T.; Moribe, M.; Oyama, Y.; Niinae, M. Mechanism of nitrate reduction by zero-valent iron: equilibrium and kinetics studies. *Chem. Eng. J.* **2012**, *183*, 271−277.
(54) Choe, S.; Liljestrand, H. M.; Khim, J. Nitrate reduction by zero-valent iron under different pH regimes. *Appl. Geochem.* **2004**, *19*, 335−342.
(55) Cheng, I. F.; Muftikian, R.; Fernando, Q.; Korte, N. Reduction of nitrate to ammonia by zero-valent iron. *Chemosphere* **1997**, *35*, 2689−2695.
(56) Gunawardana, B.; Singhal, N.; Swedlund, P. In *Dechlorination of Pentachlorophenol by Zero Valent Iron and Bimetals: Effect of Surface Characteristics and Bimetal Preparation Procedure*, Proceedings of the Annual International Conference on Soils, Sediments, Water and Energy, 2012; Vol. *17*, pp 68−81.
(57) Petr, M.; Šišková, K.; Machala, L.; Kašlík, J.; Šafářová, K.; Zbořil, R. In *Laser-Induced Transformations of Zero-Valent Iron Particles*, AIP Conference Proceedings, 2012; pp 47−55.
(58) Liang, L.; Guan, X.; Huang, Y.; Ma, J.; Sun, X.; Qiao, J.; Zhou, G. Efficient selenate removal by zero-valent iron in the presence of weak magnetic field. *Sep. Purif. Technol.* **2015**, *156*, 1064−1072.
(59) Henderson, A. D.; Demond, A. H. Long-term performance of zero-valent iron permeable reactive barriers: a critical review. *Environ. Eng. Sci.* **2007**, *24*, 401−423.

DOI: 10.1021/acsomega.6b00382
ACS Omega 2017, 2, 1513−1522